Lgd regulates ESCRT-III complex accumulation at multivesicular endosomes to control intralumenal vesicle formation

Aryel L. Clarke, Molly M. Lettman, and Anjon Audhya*
Department of Biomolecular Chemistry, University of Wisconsin School of Medicine and Public Health, Madison, WI 53705

ABSTRACT **Membrane remodeling mediated by heteropolymeric filaments composed of ESCRT-III subunits is an essential process that occurs at a variety of organelles to maintain cellular homeostasis. Members of the evolutionarily conserved Lgd/CC2D1 protein family have been suggested to regulate ESCRT-III polymer assembly, although their specific roles, particularly in vivo, remain unclear. Using the *Caenorhabditis elegans* early embryo as a model system, we show that Lgd/CC2D1 localizes to endosomal membranes, and its loss impairs endolysosomal cargo sorting and degradation. At the ultrastructural level, the absence of Lgd/CC2D1 results in the accumulation of enlarged endosomal compartments that contain a reduced number of intralumenal vesicles (ILVs). However, unlike aberrant endosome morphology caused by depletion of other ESCRT components, ILV size is only modestly altered in embryos lacking Lgd/CC2D1. Instead, loss of Lgd/CC2D1 impairs normal accumulation of ESCRT-III on endosomal membranes, likely slowing the kinetics of ILV formation. Together, our findings suggest a role for Lgd/CC2D1 in the recruitment and/or stable assembly of ESCRT-III subunits on endosomal membranes to facilitate efficient ILV biogenesis.**

Monitoring Editor
Mary Munson
University of Massachusetts

Received: Aug 16, 2022
Revised: Oct 13, 2022
Accepted: Oct 18, 2022

INTRODUCTION

The endosomal sorting complex required for transport (ESCRT) machinery has been implicated in membrane remodeling events at numerous intracellular sites, including endosomes, lysosomes, autophagosomes, plasma membrane, endoplasmic reticulum, and the nuclear envelope (Gatta and Carlton, 2019; Vietri *et al.*, 2020; Olmos, 2022). In particular, ESCRT-III complexes facilitate both membrane bending and scission, likely through their ability to form dynamic filaments that are capable of binding to lipid bilayers with high affinity, while simultaneously undergoing constriction (Pfitzner *et al.*, 2021; Migliano *et al.*, 2022). Unlike other molecular machines that promote membrane severing reactions, ESCRT-III has been suggested to act in two distinct orientations. At multivesicular endosomes (MVEs), ESCRT-III functions within the necks of nascent intralumenal vesicles (ILVs) to mediate their narrowing, eventually resulting in the deposition of ILVs into the endosome lumen for degradation (Frankel and Audhya, 2018). In a similar manner, recruitment of ESCRT-III to small holes in the plasma membrane created by extracellular damage enables lipid bilayer resealing and synchronized shedding of wounded membrane away from the cytoplasm (Jimenez *et al.*, 2014; Zhen *et al.*, 2021). Acting in an opposite orientation, ESCRT-III has also been implicated in the fission of membrane tubules, both on endosomes and the inner nuclear membrane, which are released into the cytoplasm and nucleoplasm, respectively (Allison *et al.*, 2013; McCullough *et al.*, 2015; Shankar *et al.*, 2022). How the recruitment and dynamics of ESCRT-III complexes are regulated at these different sites remains poorly understood, but likely relies upon upstream components of the ESCRT machinery, as well as accessory factors that have been shown to interact with ESCRT-III subunits (Olmos, 2022).

This article was published online ahead of print in MBoC in Press (http://www.molbiolcell.org/cgi/doi/10.1091/mbc.E22-08-0342) on October 26, 2022.

The authors declare no conflicts of interest.

Author contributions: A.L.C., M.M.L., and A.A. designed the research; A.L.C. and M.M.L. performed the research; A.L.C. and A.A. contributed the reagents/analytic tools; A.L.C., M.M.L., and A.A. analyzed the data; and A.L.C. and A.A. wrote the paper.

*Address correspondence to: Anjon Audhya (audhya@wisc.edu).

Abbreviations used: DM14, *Drosophila melanogaster*-14; DOPC, 1,2-dioleoyl-sn-glycero-3-phosphocholine; ESCRT, endosomal sorting complex required for transport; GST, glutathione *S*-transferase; ILV, intralumenal vesicle; MVE, multivesicular endosome.

In mammals, 12 ESCRT-III subunits (CHMP1A-CHMP7 and Ist1) have been identified, some of which possess overlapping roles at membrane remodeling sites. All exhibit structural similarities to one another, including the presence of multiple alpha helices, which have been shown to mediate homo- and heteropolymerization between individual subunits. In some cases, regulation of this assembly process has been suggested to rely on conformational changes that expose binding interfaces (Olmos, 2022; Migliano *et al*., 2022). As an example, inactive CHMP3 appears to exist in a closed state, where five of its alpha helices are packed against one another to prevent polymerization (Muziol *et al*., 2006; Lata *et al*., 2008). Transition to an open conformation relieves autoinhibition, enabling interaction with CHMP2 family members (Bajorek *et al*., 2009). Repeating units of CHMP2-CHMP3 heterodimers coassemble to form helical filaments on lipid bilayers, which can additionally interact with other ESCRT-III polymers, as well as the Vps4 ATPase, to ultimately drive membrane remodeling (Mierzwa *et al*., 2017; Bertin *et al*., 2020; Alqabandi *et al*., 2021; Azad *et al*., 2022). However, it remains unknown how conformational changes in individual ESCRT-III subunits are triggered to promote this cascade of events, nor is it well understood how their local concentrations are maintained at membrane surfaces to sustain progressive bilayer bending.

An alternative model suggests that ESCRT-III subunits exist in a dynamic equilibrium between open and closed states and leverage membrane binding and/or interactions with other factors to stimulate polymerization, while precocious filament assembly at inappropriate sites including the cytoplasm is prevented by a distinct set of regulators (Schuh *et al*., 2015; Tang *et al*., 2016; McMillan *et al*., 2017; Pfitzner *et al*., 2021). In particular, members of the conserved Lgd/CC2D1 (Lgd) family have been demonstrated to bind directly to CHMP4 isoforms, occluding the interface used normally to form homopolymers, without impacting their conformational states (Martinelli *et al*., 2012; McMillan *et al*., 2017; Baeumers *et al*., 2020). All Lgd proteins exhibit a similar architecture, with a series of DM14 (*Drosophila melanogaster*-14) motifs in their amino termini, which bind to a subset of ESCRT-III subunits, followed by a C2 domain that directs localization and stability (Gallagher and Knoblich, 2006; Drusenheimer *et al*., 2015; McMillan *et al*., 2017; Baeumers *et al*., 2022). Loss of function mutations in Lgd cause defects in endosomal cargo sorting, leading to lethality at the early pupal stage in *Drosophila*, which has been attributed, at least in part, to excessive activation of the Notch signaling pathway (Childress *et al*., 2006; Gallagher and Knoblich, 2006; Jaekel and Klein, 2006). Notably, overexpression of CHMP4 could partially rescue this phenotype, enabling animals to reach adulthood, although the mechanism underlying this suppression remains unclear (Baeumers *et al*., 2020). In mammals, simultaneous deletion of both genes encoding Lgd isoforms (CC2D1A and CC2D1B) causes early embryo lethality, and depletion studies indicate that they possess partially overlapping roles in regulating degradative cargo sorting within the endolysosomal system (Zhao *et al*., 2011; Drusenheimer *et al*., 2015; Deshar *et al*., 2016; Zamarbide *et al*., 2018). Additionally, CC2D1B has also been shown to regulate the timing of ESCRT-III assembly at the nuclear envelope as it reforms following mitosis. Specifically, loss of CC2D1B results in the premature polymerization of CHMP4 protomers at gaps in the nuclear envelope, leading to defects in its morphology and function (Ventimiglia *et al*., 2018). Together, these findings suggest that Lgd isoforms serve as molecular timers for ESCRT-III filament formation, helping to ensure the proper spatiotemporal activity of ESCRT-mediated membrane remodeling, although our mechanistic understanding of this regulatory role remains incomplete.

Here, we take advantage of the newly fertilized *Caenorhabditis elegans* zygote as a model system to further define the roles of Lgd in regulating ESCRT-III assembly and function. We demonstrate that Lgd localizes to early endosomes that harbor components of the ESCRT machinery rapidly after the oocyte-to-embryo transition, when de novo MVE biogenesis is initiated (Frankel *et al*., 2017). Additionally, similar to prior findings (Baeumers *et al*., 2020), we find that loss of Lgd slows the rate of degradative cargo sorting and reduces the kinetics of ILV biogenesis, resulting in the dilation of endosomes. Surprisingly, the few ILVs that form in the absence of Lgd are morphologically similar to those found in control animals, exhibiting only a modest increase in diameter, suggesting that ESCRT-III function remains largely intact under these conditions. However, we find that loss of Lgd reduces the concentration of CHMP4 on endosomes, providing a potential explanation for the kinetic delay in cargo degradation. Our data support a model in which Lgd acts to stabilize levels of CHMP4 at endosomal microdomains from which ILV formation occurs.

RESULTS

Lgd localizes to endosomes following the oocyte-to-embryo transition

Based on sequence analysis, the nematode *C. elegans* expresses a single member of the Lgd/CC2D1 protein family that is encoded by Y37H9A.3, which we refer to as Lgd. To determine its distribution during early development, we used CRISPR/Cas9-mediated genome editing to append a GFP tag onto the amino terminus of the endogenous protein. Live imaging of the resulting strain (PHX1889) using confocal microscopy revealed a mainly cytoplasmic localization of GFP-Lgd, although soon after fertilization, we found that it accumulated at numerous punctate structures that were highly dynamic near the periphery of zygotes, which was reminiscent of the distribution of early endosomes (Figure 1A and Supplemental Video 1; Wang and Audhya, 2014). To investigate this idea further, we examined the relative localizations of Lgd and the Rab5 GTPase, which marks early endosomes (Chavrier *et al*., 1990), and found that on average, more than 50% of Lgd-positive structures also harbored Rab5 (Figure 1, B and C). These data indicate that Lgd is at least in part an endosomal protein.

Early-acting components of the ESCRT machinery, including the ESCRT-I subunit Tsg101, that function upstream of ESCRT-III in the formation of MVEs similarly associate with Rab5-positive endosomes (Supplemental Figure S1, A and B; Audhya *et al*., 2007a). To examine the degree of overlap between Lgd and the ESCRT machinery, we generated animals coexpressing GFP-Lgd and mCherry-STAM, components of the ESCRT-0 complex. On average, we found that Lgd colocalizes with STAM more than 60% of the time, consistent with a role for Lgd in regulating ESCRT activity on endosomes (Figure 1, D and E). These findings raised the question of whether the ESCRT machinery itself may be involved in recruiting Lgd to membranes. To test this possibility, we conducted a series of RNA interference (RNAi)–mediated depletion studies targeting key components of the ESCRT-0, -I, -II, and -III complexes, as well as the Vps4 ATPase. While reduced levels of late-acting ESCRT components (ESCRT-II, ESCRT-III, and Vps4) failed to disrupt targeting of Lgd to endosomes harboring the ESCRT-0 subunit STAM, depletion of ESCRT-0 (Hrs) or ESCRT-I (Tsg101) significantly reduced the ability of Lgd to accumulate on endosomal membranes (Figure 2, A–D). Because depletion of Hrs prevents recruitment of STAM onto endosomes (Bache *et al*., 2003), we used a mCherry fusion to Rab5 to mark them under this particular condition (Figure 2, C and D). Overall, our data suggest that Lgd partially depends upon the early-acting ESCRT complexes for its

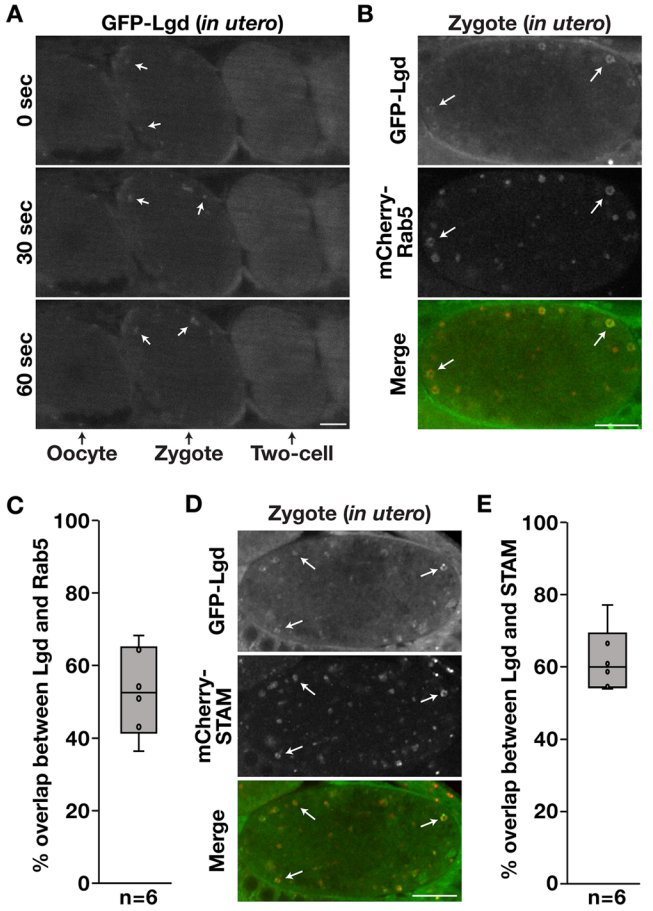

FIGURE 1: Lgd localizes to endosomes during early *C. elegans* embryogenesis. (A) Representative images taken in utero of animals natively expressing a GFP fusion to Lgd using confocal microscopy are shown at 30-s intervals ($n = 6$ animals). Bar, 10 µm.
(B, D) Representative images of zygotes coexpressing a GFP fusion to Lgd and a mCherry fusion to Rab5 (B) or STAM (D) were acquired live using confocal microscopy ($n = 6$ animals each). Bars, 10 µm.
(C, E) Quantification showing the percentage of Lgd-labeled structures that also harbor Rab5 (C) or STAM (E), calculated using Imaris.

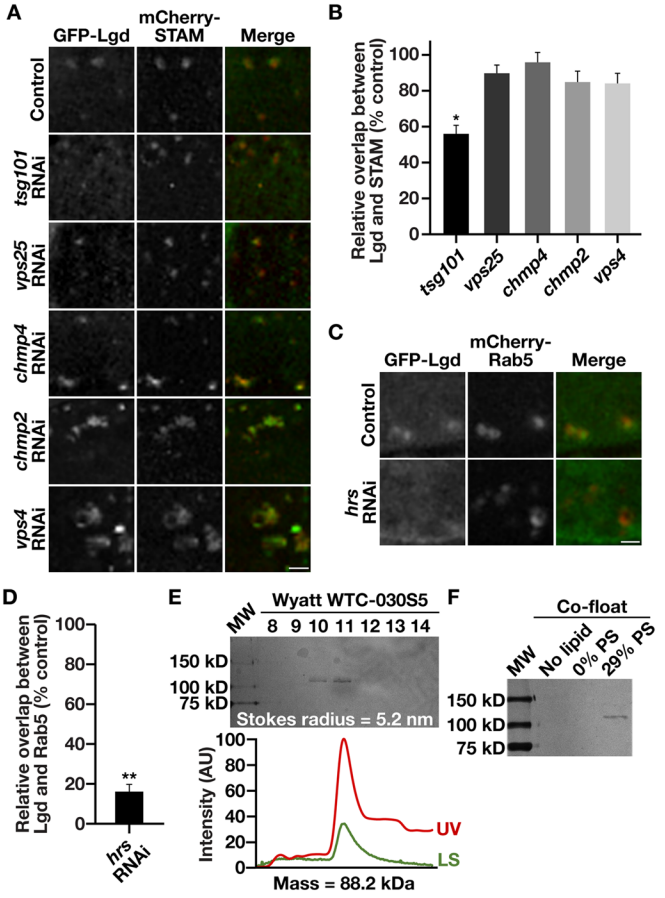

FIGURE 2: Lgd localization to endosomes is dependent on multiple factors. (A, C) Representative images of zygotes coexpressing a GFP fusion to Lgd and a mCherry fusion to STAM (A) or Rab5 (C) were acquired live using confocal microscopy (n = more than five animals each; zoomed portions of embryos are shown), in the presence and absence of various ESCRT proteins. Bar, 2 µm. (B, D) Quantification showing the relative level of overlap between Lgd and STAM (B) or Rab5 (D) under various depletion conditions as compared with control animals. **, $p < 0.01$ and *, $p < 0.05$, based on a t test (D) or an ANOVA followed by a Tukey post hoc test (B). (E) Purified recombinant Lgd was separated over a Wyatt gel filtration column coupled to a multiangle light-scattering system and fractions were separated by SDS–PAGE, followed by silver staining, to calculate its Stokes radius (top). UV absorbance (red) and light-scattering (green) profiles are also shown (bottom), which were used to calculate the molecular mass of Lgd ($n = 3$). (F) Recombinant Lgd (4 µM) was resuspended in a buffer containing Accudenz in the presence or absence of liposomes with two distinct lipid compositions and subjected to centrifugation. Protein–lipid complexes that floated to the surface were recovered by hand and subjected to SDS–PAGE, followed by silver staining ($n = 3$).

localization, but it retains an ability to associate with endosomes even in their absence, arguing that additional factors, such as phospholipids that have been suggested to associate with its C2 domain (Gallagher and Knoblich, 2006), are also involved in directing Lgd to these compartments (Figure 2, A–D). Consistent with this idea, we found that recombinant Lgd, which forms elongated monomers in solution (Figure 2E), binds directly to liposomes in vitro, in a manner that is dependent on the presence of acidic phospholipids, which are abundant in early endosomes (Figure 2F; Arumugam and Kaur, 2017).

Lgd associates with the nuclear envelope during mitosis

Notably, following penetrant depletion of the ESCRT-III subunit CHMP4, we found that Lgd hyperaccumulates on the nuclear envelopes of daughter cells (Figure 3A). Additionally, upon closer inspection of control embryos, we found that Lgd associates weakly with the periphery of the nucleus as the nuclear envelope begins to disassemble ahead of each mitotic division (Figure 3, B and C). We speculated that exposure to CHMP7, which we demonstrated previously to localize to the inner nuclear membrane during interphase in *C. elegans* embryos (Shankar *et al.*, 2022), enables transient recruitment of Lgd during nuclear envelope breakdown. Consistent with this idea, in the absence of CHMP7, Lgd accumulation at the nuclear periphery before mitosis was dramatically reduced (Figure 3, B and C). In addition, during nuclear envelope reformation following anaphase onset, Lgd was again found to associate transiently with the nuclear periphery in a manner dependent on CHMP7 (Figure 3D). To determine whether a direct interaction exists between Lgd and CHMP7, we conducted a series of GST pull-down assays, which revealed that Lgd binds CHMP7 specifically through its carboxyl-terminal ESCRT-III-like region (Figure 3E), similar to their mammalian

homologues (Ventimiglia *et al.*, 2018). We additionally found that Lgd binds directly to the *C. elegans* CHMP4 isoform (Supplemental Figure S1C), also consistent with previous studies (Martinelli *et al.*, 2012; McMillan *et al.*, 2017). However, we failed to detect interactions between Lgd and any other ESCRT-III subunit (Supplemental Figure S1D). Taken together, our findings suggest that binding to CHMP4 facilitates retention of Lgd within the cytoplasm. Moreover, in the absence of CHMP4, an interaction with CHMP7 drives redistribution of Lgd to the inner nuclear membrane. Strikingly, deletion of CHMP7 prevents targeting of Lgd to the nuclear envelope, even when CHMP4 levels are reduced via RNAi. Instead, under these conditions, Lgd accumulates at the plasma membrane, suggesting that additional binding partners for Lgd likely exist there (Supplemental Figure S1E).

Lgd is required for rapid ESCRT-mediated cargo degradation

To further investigate the role of Lgd in embryonic development, we used CRISPR/Cas9-mediated editing to create a deletion allele (*hz24*), which lacks coding regions for all four of its DM14 motifs, as well as a significant portion of its C2 domain (Supplemental Figure S1F). Animals heterozygous for this mutation were allowed to propagate under normal feeding conditions, which revealed that ~25% of all progeny failed to mature beyond the L1 larval stage. Sequencing results indicated that these developmentally arrested animals were homozygous for the deletion allele. We also examined growth under a second feeding condition, using bacterial strain HT115 as opposed to OP50 as a food source. To our surprise, this relatively modest change enabled homozygous mutant animals to reach adulthood, which was confirmed using immunoblot analysis (Figure 4A). However, homozygous mutant hermaphrodites were all sterile, exhibiting a defect in spermatogenesis, similar to a phenotype observed previously in animals lacking the ESCRT-0 subunit STAM (Govindan *et al.*, 2006). By mating these mutant hermaphrodites with control males, we were able to study the first zygotic divisions in the absence of Lgd, as expression of the male-derived genome does not initiate for several embryonic cell cycles (Seydoux and Dunn, 1997).

Previous studies have identified numerous ubiquitin-modified, membrane-associated cargoes that are substrates for ESCRT-dependent sorting into MVEs (Raiborg *et al.*, 2003). In *C. elegans* embryos, a GFP fusion to caveolin-1 (Cav1) serves as an ideal model cargo, with inactivation of GFP fluorescence serving as a proxy for the timing of ESCRT-mediated internalization into the lumen of acidified endosomes (Sato *et al.*, 2006; Audhya *et al.*, 2007a; Frankel *et al.*, 2017). To determine how loss of Lgd affects endosomal cargo sorting, we examined the rate at which Cav1 fluorescence was terminated during early embryogenesis in control and mutant animals. Our findings consistently showed that the absence of Lgd dramatically slowed the kinetics of Cav1 degradation relative to control (Figure 4B; 10/10 animals lacking Lgd exhibited Cav1 fluorescence at the four-cell stage, while 0/10 control animals exhibited this phenotype). Instead, Cav1 localized to enlarged membrane compartments in mutant animals, similar to those seen in animals depleted of CHMP4 (Frankel *et al.*, 2017).

To confirm the identity of the sites where Cav1 accumulated in embryos lacking Lgd, we conducted a series of immunofluorescence studies. Consistent with the idea that the loss of Lgd impairs endosomal protein sorting, we found that Cav1 colocalized with components of the ESCRT-0 and ESCRT-I complexes on abnormally large endosomes in mutant animals (Figure 4, C and D). In contrast, we failed to identify CHMP4 at the majority of these sites

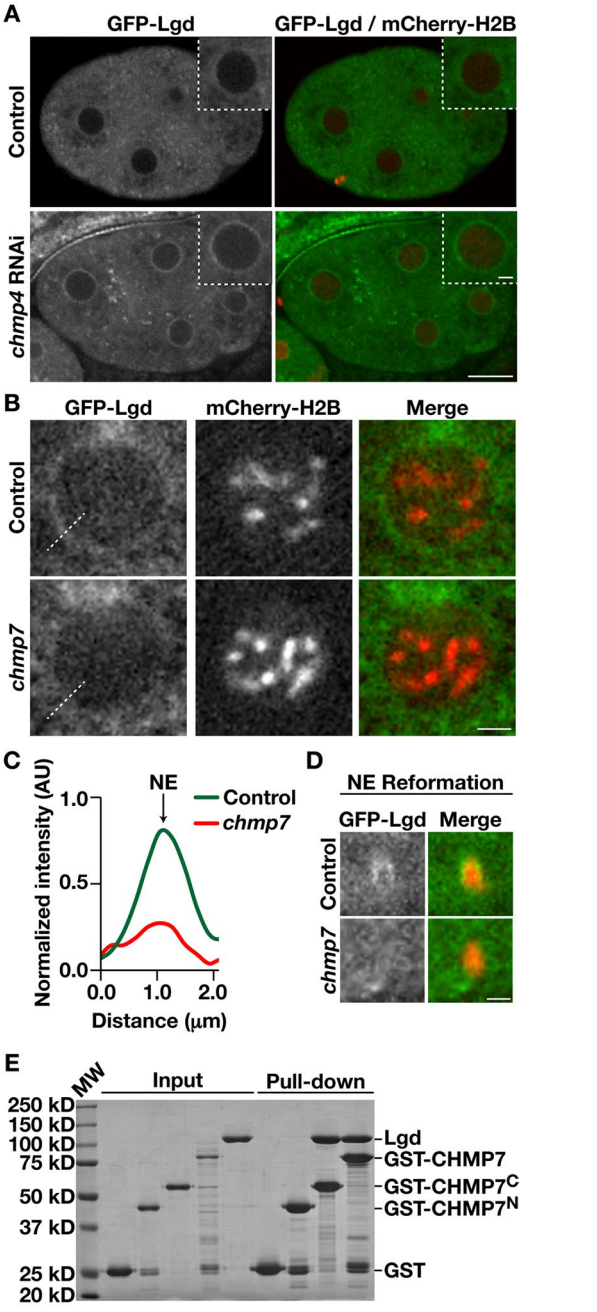

FIGURE 3: Lgd binds to CHMP7 at the inner nuclear membrane. (A) Representative images of four-cell stage embryos coexpressing a GFP fusion to Lgd and an mCherry fusion to histone H2B were imaged live using confocal microscopy in the presence and absence of CHMP4 ($n = 5$ animals each). Zoomed regions of nuclei are also shown. Bar, 10 μm; inset bar, 2 μm. (B, D) Representative images of embryos (zoomed to visualize nuclei) coexpressing a GFP fusion to Lgd and an mCherry fusion to histone H2B during nuclear envelope breakdown (B) and nuclear envelope reformation (D), in the presence (top) and absence (bottom) of CHMP7. Bars, 2 μm. (C) Linescan analysis showing the fluorescence intensity of GFP-Lgd along the dashed lines shown in panel B in the presence and absence of CHMP7. (E) GST and GST fusions to CHMP7 (full-length or fragments) bound to glutathione agarose were incubated with full-length recombinant Lgd, and after extensive washing, proteins were eluted and separated by SDS–PAGE followed by staining using Coomassie ($n = 3$). Note that Lgd associates with the CHMP7 carboxyl-terminal domain ($CHMP7^C$), but not its amino-terminal domain ($CHMP7^N$).

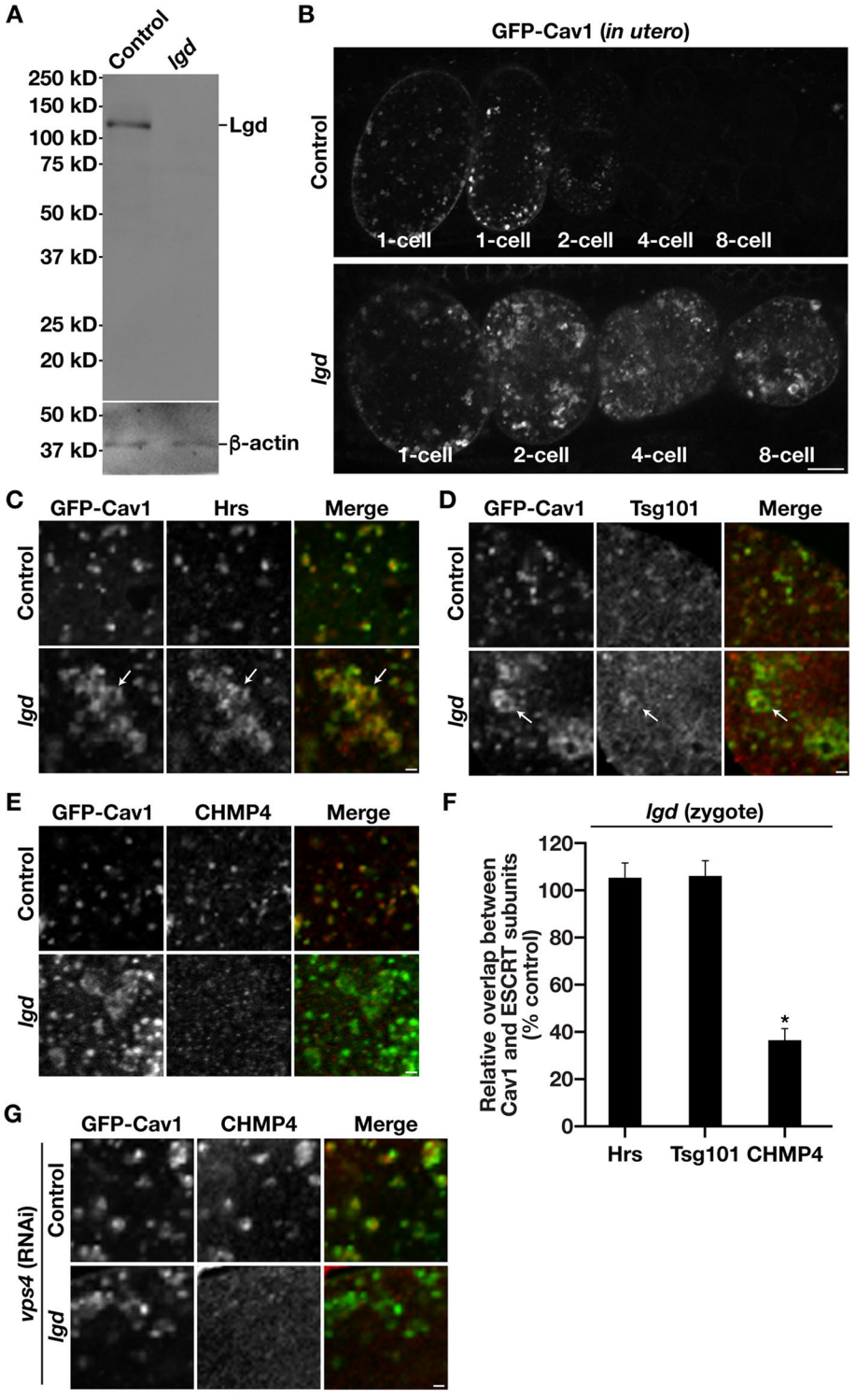

FIGURE 4: Lgd regulates CHMP4 recruitment to MVEs. (A) Representative immunoblot using antibodies directed against Lgd (top) or β-actin (bottom) of extracts generated from control and *lgd* mutant animals, following separation by SDS–PAGE ($n = 3$). (B) Representative images taken in utero of control and *lgd* mutant animals expressing a GFP fusion to Cav1 using confocal microscopy are shown ($n = 10$ animals each). Bar, 10 μm. (C–E) Representative images of control and *lgd* mutant zygotes expressing a GFP fusion to Cav1 and immunostained using antibodies directed against Hrs (C), Tsg101 (D), or CHMP4 (E) are shown ($n = 5$ animals each; zoomed portions of embryos are shown). Bars, 2 μm. (F) Quantification showing the relative level of overlap between Cav1 and various ESCRT subunits in animals lacking Lgd as compared with control animals. *, $p < 0.05$, based on an ANOVA followed by a Tukey post hoc test. (G) Representative images of control and *lgd* mutant zygotes expressing a GFP fusion to Cav1 and immunostained using antibodies directed against CHMP4 are shown following depletion of Vps4 ($n = 5$ animals each; zoomed portions of embryos are shown). Bar, 2 μm.

(Figure 4, E and F), suggesting a defect in its recruitment to endosomal microdomains in the absence of Lgd. Even under conditions where we codepleted Vps4, which blocks recycling of ESCRT-III subunits from membranes (McCullough *et al.*, 2018), we did not find that CHMP4 hyperaccumulated at the abnormally swollen endosomes that form in embryos lacking Lgd (Figure 4G). Instead, CHMP4 remained largely cytoplasmic under these conditions. Our findings suggest that Lgd functions in the stable recruitment of CHMP4 to endosomes, as opposed to acting only as an inhibitor of CHMP4 polymerization.

Lgd regulates the formation of ILVs

To better define the impact of removing Lgd on the formation of MVEs, we conducted high-pressure freezing of intact control and mutant animals, and following freeze substitution and embedding in plastic, negatively stained thin sections of early one-cell stage embryos were analyzed by electron microscopy. These studies revealed significant differences in the sizes of endosomes and ILVs that form in the presence and absence of Lgd (Figure 5, A–D). Specifically, we found that the average diameter of endosomes increased by more than 30% when Lgd was eliminated, with a concomitant decrease in the number of ILVs that were identified within them (Figure 5, B and C). The vast majority of endosomes in embryos lacking Lgd harbored no internal vesicles (more than 75%), with the remainder containing fewer than five ILVs in any individual section (Figure 5E). In contrast, analysis of control embryos showed most MVEs contained at least one ILV (more than 75%), and greater than 30% possessed more than six ILVs, a population that was entirely absent in mutant embryos (Figure 5E).

Rigorous analysis of ILVs demonstrated that loss of Lgd causes an ~20% increase in their diameter (Figure 5B). Our previous studies similarly showed that partial depletion of CHMP4 also results in the formation of larger ILVs (Frankel *et al.*, 2017), consistent with a model in which Lgd facilitates its stable recruitment to the endosomal limiting membrane (Figure 6). Together, our findings suggest that Lgd-mediated regulation of CHMP4 accumulation promotes efficient ILV formation at MVEs to sort and ultimately degrade cargoes.

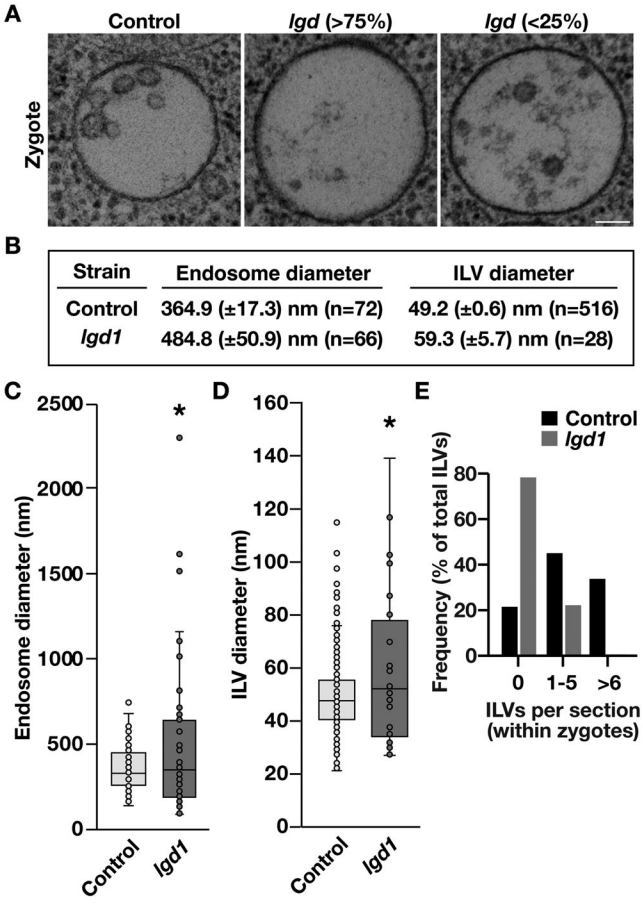

FIGURE 5: Loss of Lgd impairs ILV formation within MVEs. (A) Representative images of MVEs in control and *lgd* mutant zygotes following negative staining electron microscopy (n = more than 60 MVEs, each). Bar, 100 nm. (B–D) Quantification of MVE (C) and ILV (D) diameter in control and *lgd* mutant zygotes, including a table with averages (B). *, $p < 0.05$, based on a t test. (E) Histogram showing the relative number of ILVs identified in thin sections from control and *lgd* mutant zygotes.

DISCUSSION

Because the first descriptions of the ESCRT machinery were published more than two decades ago (Katzmann *et al.*, 2001; Babst *et al.*, 2002a,b), substantial efforts have been invested to define the structure and function of individual subunits and complexes to understand how its ability to manipulate membranes is achieved. We now have a comprehensive list of the key players involved, including broad consensus in the field that the ESCRT-III complex promotes membrane bending and scission (Olmos, 2022). However, at a mechanistic level, how ESCRT-III assembly on membranes is orchestrated and properly tuned remains unclear. Given the large number of membrane remodeling processes in which ESCRT-III has been implicated, there likely exist numerous forms of regulation to ensure its timely action at each site. Our studies highlight the importance of ESCRT-III regulation at endosomes, which involves the CHMP4-binding protein Lgd. Despite the ability of Lgd to obscure the key interface necessary for CHMP4 homopolymerization, we find that it is surprisingly required for promoting CHMP4 association with the endosomal limiting membrane, potentially by maintaining a local pool of subunits for rapid assembly necessary to scaffold the membrane bending process to create ILVs.

Although several studies have attempted to specify the distribution of Lgd in cells, most have depended upon the use of overexpression, making it difficult to resolve Lgd association with cellular membranes above its presence in the cytoplasm (Reiff *et al.*, 2021). Recently, by driving overexpression under its native promoter in *Drosophila*, a small fraction of Lgd was found to associate with endosomes (Baeumers *et al.*, 2020). In contrast, by leveraging CRISPR/Cas9-mediated genome editing, we have found that a substantial fraction of Lgd localizes with the early endosome markers Rab5 and STAM in one-cell stage *C. elegans* embryos. At this stage of development, a large number of MVEs are generated de novo, as membrane proteins associated with the oocyte plasma membrane must be rapidly down-regulated and replaced (Wang and Audhya, 2014). Elevated flux through the ESCRT pathway during this period likely enhanced our ability to resolve Lgd with other components of the ESCRT machinery at endosomes. Similarly, Lgd association with the nuclear envelope has been challenging to resolve under normal conditions, due to its transient accumulation there during mitosis (Ventimiglia *et al.*, 2018). Strikingly, by depleting CHMP4, we found that Lgd accumulated in a CHMP7-dependent manner at the inner nuclear envelope during interphase. This was surprising, because several lines of evidence suggest that Lgd can associate with both CHMP7 and CHMP4 simultaneously (McMillan *et al.*, 2017; Ventimiglia *et al.*, 2018). The necessity to deplete CHMP4 to visualize stable localization of Lgd to the nuclear envelope in *C. elegans* embryos suggests that in vivo, there exists competition between ESCRT-III subunits for binding to Lgd, at least during mitosis, when CHMP7 enters the cytoplasm and localizes throughout the endoplasmic reticulum (Vietri *et al.*, 2015; Olmos *et al.*, 2016). Further studies will be necessary to understand how Lgd binding to different ESCRT-III factors is regulated, although our biochemical studies suggest that only CHMP4 and CHMP7 are substrates of Lgd.

An additional localization determinant for Lgd lies within its carboxyl-terminal C2 domain. Several studies have shown that the C2 domain of Lgd is necessary for its function and ability to bind membranes, both at endosomes and the nuclear envelope (Gallagher and Knoblich, 2006; Troost *et al.*, 2012; Ventimiglia *et al.*, 2018). Consistent with these studies, we found that *C. elegans* Lgd minimally requires the presence of acidic phospholipids to bind liposomes in vitro, indicative that the role of the C2 domain in membrane binding is likely conserved. Additionally, our depletion studies suggest that Lgd remains capable, albeit weakly, of binding to endosomes, even when upstream components of the ESCRT machinery are absent. These studies suggest that coincident detection of protein- and lipid-binding partners, a common theme in phosphoinositide signaling pathways (Carlton and Cullen, 2005), are necessary to specify the membranes on which Lgd acts. By leveraging coincident detection, Lgd may achieve highly restricted localization patterns in cells, preventing its action at other sites, which could interfere with ESCRT function as opposed to facilitating it. Notably, when both CHMP4 and CHMP7 are absent, Lgd is redistributed in part to the plasma membrane. These studies suggest that additional, potentially lower affinity binding partners for Lgd exist, which await discovery.

Based on previous studies, in concert with our current findings, a role for Lgd at MVEs to regulate degradative cargo sorting via stimulation of ILV biogenesis is clear (Baeumers *et al.*, 2020). Our data show that normal CHMP4 accumulation at the limiting membrane requires Lgd, suggesting that targeting of ESCRT-III subunits likely relies on additional factors beyond canonical upstream components of the ESCRT machinery. Although several mechanisms exist to promote CHMP4 accumulation on membranes, including key roles for

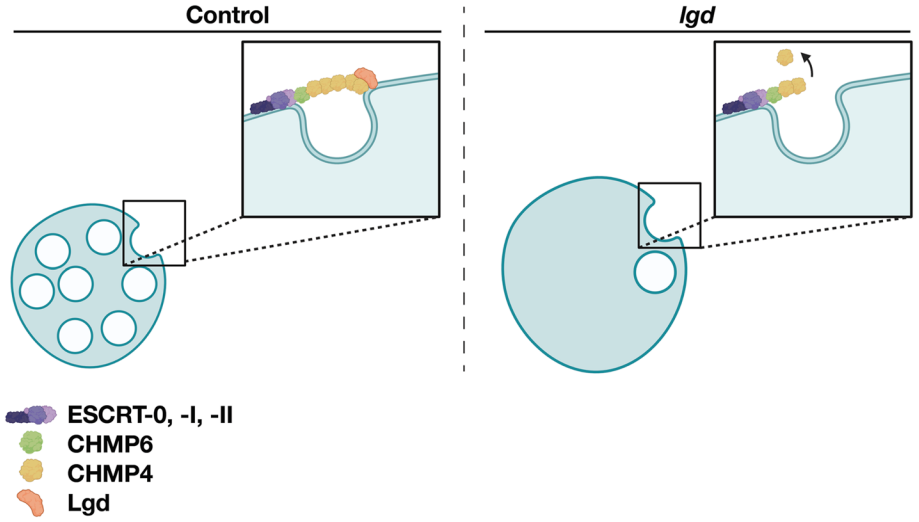

FIGURE 6: Model highlighting a role for Lgd during ILV formation. Based on our findings, we propose that Lgd functions to stabilize CHMP4 at the limiting membrane of endosomes to facilitate ILV formation (left). In the absence of Lgd, CHMP4 recruitment to MVEs is diminished, slowing the biogenesis of ILVs and decreasing the rate of cargo degradation (right).

CHMP6 at MVEs, CHMP7 at the nuclear envelope, and ALIX at sites of HIV budding, the efficiencies of these processes may be further enhanced by molecules like Lgd (Vietri *et al.*, 2020). One possibility is that a low concentration of Lgd present on cellular membranes serves to maintain a local pool of CHMP4 subunits, which can rapidly coassemble into spiral filaments upon demand. In light of our prior work demonstrating that nearly 800 subunits of CHMP4 can homopolymerize into flat spiral filaments (Shen *et al.*, 2014), it is perhaps unsurprising that additional regulatory mechanisms act in cells to retain individual CHMP4 protomers at sites of filament assembly. In the absence of Lgd, recruitment of CHMP4 to MVEs is reduced, but not eliminated, compromising the rate of ILV formation. Under conditions where rapid down-regulation of membrane-bound receptors is necessary, including embryonic and larval development, the loss of Lgd is lethal, as has been observed in mice, *Drosophila*, and now in *C. elegans* (Reiff *et al.*, 2021). Future studies aimed at testing the idea of Lgd serving as a "concentrator" for CHMP4 on membranes will be important to fully understand the mechanisms underlying regulation of ESCRT-mediated membrane remodeling.

MATERIALS AND METHODS

CRISPR/Cas9-mediated genome editing and RNAi

Genome editing to create a deletion within *C. elegans* Lgd (*hz24*) was carried out in the Bristol strain N2 (or a derivative) as described previously (Paix *et al.*, 2015). The following pair of guide RNAs was used to generate the deletion allele, which created breakpoints between exons 1 and 2 and between exons 8 and 9, followed by nonhomologous end joining: 5′-ACAAUUUACCCCUAUUGAGC-3′ and 5′-AUUUUUUAAAUAUCGACCUU-3′. Generation of an allele encoding an amino-terminal GFP fusion to endogenous Lgd (*syb1889*) was outsourced (SunyBiotech). Specifically, the sequence of a codon-optimized version of GFP (S65C) for expression in *C. elegans* (including introns) was inserted immediately downstream from the start codon of Lgd, leveraging the following guide RNA: 5′-GAUAUUGAUAAUCAAAUGUA-3′. All other strains used have been characterized previously (McNally *et al.*, 2006; Sato *et al.*, 2006; Audhya *et al.*, 2007b; Frankel *et al.*, 2017). Standard genetic crosses were performed to combine alleles, and all strains were maintained at either 20°C or 15°C. Templates for generating double-stranded RNAs used in RNAi experiments were synthesized by PCR using N2 genomic DNA or cDNA. Depletion studies were conducted as described previously (Frankel *et al.*, 2017).

Fluorescence and electron microscopy imaging studies

Confocal imaging was conducted either using a swept-field confocal scanhead (distributed by Bruker) mounted onto a Nikon Eclipse Ti-E microscope stand, equipped with a 60× Planapo oil immersion objective and a CoolSNAP HQ2 CCD camera or a Yokogawa W1 confocal scanhead mounted onto a Nikon Ti2 microscope with a Hamamatsu Orca Flash 4 camera. For immunofluorescence studies, embryos were fixed using cold methanol and stained as described previously (Crittenden and Kimble, 2009; Frankel *et al.*, 2017). For live imaging, animals were mounted onto 10% agarose pads and imaged under minimal compression in polystyrene beads (Polysciences; 2.5% by volume, 0.1 μm diameter). Fluorescence intensity measurements and colocalization analyses were performed using Imaris.

For electron microscopy, worms were loaded into 100-μm deep sample holders (Technotrade, Manchester, NH) coated with 1-hexadecene, and a suspension of bacteria was used as a cryoprotectant. High-pressure freezing was carried out using a Leica EM ICE system. After freezing, samples were substituted into a solution of 1% OsO_4 and 1% H_2O in acetone, as described previously (Shankar *et al.*, 2022), followed by centrifugation into increasing concentrations of epoxy EMbed 812 resin (Electron Microscopy Sciences, Hatfield, PA). Animals were mounted and sectioned longitudinally (~80 nm). Samples were poststained as described previously and imaged using a Philips CM120 TEM operated at 80 kV and equipped with an AMT Biosprint 12 series digital camera.

Antibody production and recombinant protein purification and analysis

Production of rabbit polyclonal antiserum directed against Lgd was outsourced (Pacific Immunology, Ramona, CA). Rabbits were immunized with a fragment of Lgd (residues 345–792), and serum was affinity purified as described previously (Audhya *et al.*, 2007a). Antibodies directed against other *C. elegans* ESCRT proteins have been described elsewhere (Mayers *et al.*, 2013; Shen *et al.*, 2014; Frankel *et al.*, 2017). All antibodies were used at a final concentration of 1 μg/ml, with the exception of Lgd antibodies (used at 10 μg/ml) and CHMP4 antibodies (used at 5 μg/ml). Antibodies directed against β-actin were obtained commercially (Sigma).

Recombinant proteins were expressed using BL21-T1R (DE3) bacteria, as described previously (Schuh *et al.*, 2015). Full-length Lgd, as well as truncation mutants, were cloned into the pET-28a vector, which encodes a cleavable 6xHis-SUMO tag at the amino terminus. Initial purifications from bacterial lysates were performed using Ni-nitrilotriacetic acid agarose, and eluted proteins were applied onto a MonoS 5/50 GL cation exchange column (Cytiva) to

increase purity. ESCRT-III subunits were expressed as GST fusion proteins and purified on glutathione agarose beads. In cases where the GST tag was cleaved, eluted proteins were applied onto an SRT-C SEC-300 size exclusion column (Sepax Technologies, Neward, DE) for further purification.

For GST pull-down assays, 100 µg of purified GST or a GST fusion protein was bound to 8 µl of glutathione agarose beads and washed extensively. A potential binding partner of 80 µg was then incubated with the beads for 1 h, followed by washing. Bound proteins were recovered by boiling in sample buffer and separated by SDS–PAGE, followed by Coomassie or silver staining. For multiangle light-scattering studies, purified protein was applied onto a size exclusion chromatography column (WTC-030S5; Wyatt Technology Corporation, Santa Barbara, CA), coupled to a three-angle light-scattering detector (miniDAWN TREOS; Wyatt Technology Corporation). Data were collected at a flow rate of 0.5 ml/min and analyzed using ASTRA software (Wyatt Technology Corporation). The Stokes radius of each protein or protein complex was calculated from its elution volume, based on the elution profiles of characterized globular standards on the Wyatt column, as described previously (Schuh *et al.*, 2015).

Liposome generation and cofloatation assays

Liposomes were generated as described previously (Schuh *et al.*, 2015; Hanna *et al.*, 2016), composed of either 1,2-dioleoyl-sn-glycero-3-phosphocholine (DOPC), 99% and 1,2-dipalmitoyl-sn-glycero-3-phosphoethanolamine-N-(lissamine rhodamine B sulfonyl) (ammonium salt) (Rho-PE), 1%, or DOPC, 70%; 1,2-dioleoyl-sn-glycero-3-phosphoserine, 29%; Rho-PE, 1%. Lipid mixtures were dried, resuspended in buffer to a final concentration of 15 mM, and subjected to extrusion through a nitrocellulose filter (Whatman) with 0.03-µm pores.

For liposome cofloatation assays, 4 µM of purified Lgd was incubated with 2 mM charged or neutral liposomes at room temperature for 30 min, then mixed with an equal volume of 80% Accudenz (Accurate Chemical and Scientific Corporation, Carle Place, NY) to form a 40% Accudenz–liposome–protein solution. 35%, 30%, and 0% Accudenz layers were added on top and centrifuged at 50,000 rpm for 2.5 h. The top 40 µl were collected and analyzed by SDS–PAGE followed by silver staining.

ACKNOWLEDGMENTS

This work was supported in part by National Institute of Health Grants no. R35 GM-134865 (to A.A.) and no. T32 GM-07215, as well as a National Science Foundation Graduate Research Fellowship (to A.L.C.). Support was also provided by the University of Wisconsin School of Medicine and Public Health Electron Microscope Core Facility and the 3D Cell Electron Microscopy Core Facility (supported by S10OD026769). The model figure presented in this article was prepared using BioRender. We thank Siyu Li and Gordon Thompson for their contributions to generating preliminary data and members of the Audhya lab for critically reading this manuscript.

REFERENCES

Allison R, Lumb JH, Fassier C, Connell JW, Ten Martin D, Seaman MN, Hazan J, Reid E (2013). An ESCRT-spastin interaction promotes fission of recycling tubules from the endosome. J Cell Biol 202, 527–543.

Alqabandi M, de Franceschi N, Maity S, Miguet N, Bally M, Roos WH, Weissenhorn W, Bassereau P, Mangenot S (2021). The ESCRT-III isoforms CHMP2A and CHMP2B display different effects on membranes upon polymerization. BMC Biol 19, 66.

Audhya A, Desai A, Oegema K (2007b). A role for Rab5 in structuring the endoplasmic reticulum. J Cell Biol 178, 43–56.

Audhya A, McLeod IX, Yates JR, Oegema K (2007a). MVB-12, a fourth subunit of metazoan ESCRT-I, functions in receptor downregulation. PLoS One 2, e956.

Arumugam S, Kaur A (2017). The lipids of the early endosomes: making multimodality work. Chembiochem 18, 1053–1060.

Azad K, Guilligay D, Boscheron C, Maity S, Franceschi ND, Sulbaran G, Effantin G, Wang H, Kleman JP, Bassereau P, *et al.* (2022). Structural basis of CHMP2A-CHMP3 ESCRT-III polymer assembly and membrane cleavage. bioRxiv 2022.04.12.487901.

Babst M, Katzmann DJ, Estepa-Sabal EJ, Meerloo T, Emr SD (2002a). Escrt-III: an endosome-associated heterooligomeric protein complex required for mvb sorting. Dev Cell 3, 271–282.

Babst M, Katzmann DJ, Snyder WB, Wendland B, Emr SD (2002b). Endosome-associated complex, ESCRT-II, recruits transport machinery for protein sorting at the multivesicular body. Dev Cell 3, 283–289.

Bache KG, Raiborg C, Mehlum A, Stenmark H (2003). STAM and Hrs are subunits of a multivalent ubiquitin-binding complex on early endosomes. J Biol Chem 278, 12513–12521.

Baeumers M, Ruhnau K, Breuer T, Pannen H, Goerlich B, Kniebel A, Haensch S, Weidtkamp-Peters S, Schmitt L, Klein T (2020). Lethal (2) giant discs (Lgd)/CC2D1 is required for the full activity of the ESCRT machinery. BMC Biol 18, 200.

Baeumers M, Schulz K, Klein T (2022). Using *Drosophila melanogaster* to analyse the human paralogs of the ESCRT-III core component Shrub/CHMP4/Snf7 and its interactions with members of the LGD/CC2D1 family. Int J Mol Sci 23, 7507.

Bajorek M, Schubert HL, McCullough J, Langelier C, Eckert DM, Stubblefield WM, Uter NT, Myszka DG, Hill CP, Sundquist WI (2009). Structural basis for ESCRT-III protein autoinhibition. Nat Struct Mol Biol 16, 754–762.

Bertin A, de Franceschi N, de la Mora E, Maity S, Alqabandi M, Miguet N, di Cicco A, Roos WH, Mangenot S, Weissenhorn W, *et al.* (2020). Human ESCRT-III polymers assemble on positively curved membranes and induce helical membrane tube formation. Nat Commun 11, 2663.

Carlton JG, Cullen PJ (2005). Coincidence detection in phosphoinositide signaling. Trends Cell Biol 15, 540–547.

Chavrier P, Parton RG, Hauri HP, Simons K, Zerial M (1990). Localization of low molecular weight GTP binding proteins to exocytic and endocytic compartments. Cell 62, 317–329.

Childress JL, Acar M, Tao C, Halder G (2006). Lethal giant discs, a novel C2-domain protein, restricts notch activation during endocytosis. Curr Biol 16, 2228–2233.

Crittenden S, Kimble J (2009). Preparation and immunolabeling of *Caenorhabditis elegans*. Cold Spring Harb Protoc pdb.prot5216.

Deshar R, Cho EB, Yoon SK, Yoon JB (2016). CC2D1A and CC2D1B regulate degradation and signaling of EGFR and TLR4. Biochem Biophys Res Commun 480, 280–287.

Drusenheimer N, Migdal B, Jäckel S, Tveriakhina L, Scheider K, Schulz K, Gröper J, Köhrer K, Klein T (2015). The mammalian orthologs of *Drosophila* Lgd, CC2D1A and CC2D1B, function in the endocytic pathway, but their individual loss of function does not affect Notch signalling. PLoS Genet 11, e1005749.

Frankel EB, Audhya A (2018). ESCRT-dependent cargo sorting at multivesicular endosomes. Semin Cell Dev Biol 74, 4–10.

Frankel EB, Shankar R, Moresco JJ, Yates JR 3rd, Volkmann N, Audhya A (2017). Ist1 regulates ESCRT-III assembly and function during multivesicular endosome biogenesis in *Caenorhabditis elegans* embryos. Nat Commun 8, 1439.

Gallagher CM, Knoblich JA (2006). The conserved c2 domain protein lethal (2) giant discs regulates protein trafficking in *Drosophila*. Dev Cell 11, 641–53.

Gatta AT, Carlton JG (2019). The ESCRT-machinery: closing holes and expanding roles. Curr Opin Cell Biol 59, 121–132.

Govindan JA, Cheng H, Harris JE, Greenstein D (2006). Galphao/i and Galphas signaling function in parallel with the MSP/Eph receptor to control meiotic diapause in *C. elegans*. Curr Biol 16, 1257–1268.

Hanna MG, Mela I, Wang L, Henderson RM, Chapman ER, Edwardson JM, Audhya A (2016). Sar1 GTPase activity is regulated by membrane curvature. J Biol Chem 291, 1014–1027.

Jaekel R, Klein T (2006). The *Drosophila* Notch inhibitor and tumor suppressor gene lethal (2) giant discs encodes a conserved regulator of endosomal trafficking. Dev Cell 11, 655–669.

Jimenez A J, Maiuri P, Lafaurie-Janvore J, Divoux S, Piel M, Perez F (2014). ESCRT machinery is required for plasma membrane repair. Science 343, 1247136.

Katzmann DJ, Babst M, Emr SD (2001). Ubiquitin-dependent sorting into the multivesicular body pathway requires the function of a conserved endosomal protein sorting complex, ESCRT-I. Cell 106, 145–155.
Lata S, Roessle M, Solomons J, Jamin M, Gottlinger HG, Svergun DI, Weissenhorn W (2008). Structural basis for autoinhibition of ESCRT-III CHMP3. J Mol Biol 378, 818–827.
Martinelli N, Hartlieb B, Usami Y, Sabin C, Dordor A, Miguet N, Avilov SV, Ribeiro E A Jr, Göttlinger H, Weissenhorn W (2012). CC2D1A is a regulator of ESCRT-III CHMP4B. J Mol Biol 419, 75–88.
Mayers J R, Wang L, Pramanik J, Johnson A, Sarkeshik A, Wang Y, Saengsawang W, Yates JR 3rd, Audhya A (2013). Regulation of ubiquitin-dependent cargo sorting by multiple endocytic adaptors at the plasma membrane. Proc Natl Acad Sci USA 110, 11857–11862.
McCullough J, Clippinger A K, Talledge N, Skowyra ML, Saunders MG, Naismith TV, Colf LA, Afonine P, Arthur C, Sundquist WI, *et al*. (2015). Structure and membrane remodeling activity of ESCRT-III helical polymers. Science 350, 1548–1551.
McCullough J, Frost A, Sundquist WI (2018). Structures, functions, and dynamics of ESCRT-III/Vps4 membrane remodeling and fission complexes. Annu Rev Cell Dev Biol 34, 85–109.
McMillan BJ, Tibbe C, Drabek AA, Seegar TC M, Blacklow SC, Klein T (2017). Structural basis for regulation of ESCRT-III complexes by Lgd. Cell Rep 19, 1750–1757.
McNally K, Audhya A, Oegema K, McNally FJ (2006). Katanin controls mitotic and meiotic spindle length. J Cell Biol 175, 881–891.
Mierzwa BE, Chiaruttini N, Redondo-Morata L, von Filseck JM, König J, Larios J, Poser I, Müller-Reichert T, Scheuring S, Roux A, *et al*. (2017). Dynamic subunit turnover in ESCRT-III assemblies is regulated by Vps4 to mediate membrane remodelling during cytokinesis. Nat Cell Biol 19, 787–798.
Migliano SM, Wenzel EM, Stenmark H (2022). Biophysical and molecular mechanisms of ESCRT functions, and their implications for disease. Curr Opin Cell Biol 75, 102062.
Muzioł T, Pineda-Molina E, Ravelli RB, Zamborlini A, Usami Y, Göttlinger H, Weissenhorn W (2006). Structural basis for budding by the ESCRT-III factor CHMP3. Dev Cell 10, 821–830.
Olmos Y (2022). The ESCRT machinery: remodeling, repairing, and sealing membranes. Membranes (Basel) 12, 633.
Olmos Y, Perdrix-Rosell A, Carlton JG (2016). Membrane binding by CHMP7 coordinates ESCRT-III-dependent nuclear envelope reformation. Curr Biol 26, 2635–2641.
Paix A, Folkmann A, Rasoloson D, Seydoux G (2015). High efficiency, homology-directed genome editing in *Caenorhabditis elegans* using CRISPR-Cas9 ribonucleoprotein complexes. Genetics 201, 47–54.
Pfitzner AK, Moser von Filseck J, Roux A (2021). Principles of membrane remodeling by dynamic ESCRT-III polymers. Trends Cell Biol 31, 856–868.
Raiborg C, Rusten TE, Stenmark H (2003). Protein sorting into multivesicular endosomes. Curr Opin Cell Biol 15, 446–455.
Reiff T, Baeumers M, Tibbe C, Klein T (2021). Unravelling of hidden secrets: the tumour suppressor lethal (2) giant discs (Lgd)/CC2D1, Notch signalling and cancer. Adv Exp Med Biol 1287, 31–46.
Sato K, Sato M, Audhya A, Oegema K, Schweinsberg P, Grant BD (2006). Dynamic regulation of caveolin-1 trafficking in the germ line and embryo of *Caenorhabditis elegans*. Mol Biol Cell 17, 3085–3094.
Schuh A L, Hanna M, Quinney K, Wang L, Sarkeshik A, Yates JR 3rd, Audhya A (2015). The VPS-20 subunit of the endosomal sorting complex ESCRT-III exhibits an open conformation in the absence of upstream activation. Biochem J 466, 625–637.
Seydoux G, Dunn MA (1997). Transcriptionally repressed germ cells lack a subpopulation of phosphorylated RNA polymerase II in early embryos of *Caenorhabditis elegans* and *Drosophila melanogaster*. Development 124, 2191–2201.
Shankar R, Lettman MM, Whisler W, Frankel EB, Audhya A (2022). The ESCRT machinery directs quality control over inner nuclear membrane architecture. Cell Rep 38, 110263.
Shen QT, Schuh AL, Zheng Y, Quinney K, Wang L, Hanna M, Mitchell JC, Otegui MS, Ahlquist P, Cui Q, *et al*. (2014). Structural analysis and modeling reveals new mechanisms governing ESCRT-III spiral filament assembly. J Cell Biol 206, 763–777.
Tang S, Buchkovich NJ, Henne WM, Banjade S, Kim YJ, Emr SD (2016). ESCRT-III activation by parallel action of ESCRT-I/II and ESCRT-0/Bro1 during MVB biogenesis. Elife 5, e15507.
Troost T, Jaeckel S, Ohlenhard N, Klein T (2012). The tumour suppressor lethal (2) giant discs is required for the function of the ESCRT-III component Shrub/CHMP4. J Cell Sci 125, 763–776.
Ventimiglia LN, Cuesta-Geijo MA, Martinelli N, Caballe A, Macheboeuf P, Miguet N, Parnham IM, Olmos Y, Carlton JG, Weissenhorn W, *et al*. (2018). CC2D1B coordinates ESCRT-III activity during the mitotic reformation of the nuclear envelope. Dev Cell 47, 547–563.e6.
Vietri M, Radulovic M, Stenmark H (2020). The many functions of ESCRTs. Nat Rev Mol Cell Biol 21, 25–42.
Vietri M, Schink KO, Campsteijn C, Wegner CS, Schultz SW, Christ L, Thoresen SB, Brech A, Raiborg C, Stenmark H (2015). Spastin and ESCRT-III coordinate mitotic spindle disassembly and nuclear envelope sealing. Nature 522, 231–235.
Wang L, Audhya A (2014). In vivo imaging of *C. elegans* endocytosis. Methods 68, 518–528.
Zamarbide M, Oaks AW, Pond HL, Adelman JS, Manzini MC (2018). Loss of the intellectual disability and autism gene Cc2d1a and its homolog Cc2d1b differentially affect spatial memory, anxiety, and hyperactivity. Front Genet 9, 65.
Zhao M, Raingo J, Chen ZJ, Kavalali ET (2011). Cc2d1a, a C2 domain containing protein linked to nonsyndromic mental retardation, controls functional maturation of central synapses. J Neurophysiol 105, 1506–1515.
Zhen Y, Radulovic M, Vietri M, Stenmark H (2021). Sealing holes in cellular membranes. EMBO J 40, e106922.